Elongated S-cone stimuli reveal the importance of the intermediate temporal filter

Baraas, Rigmor C. and Kulikowski, Janus J. and Muldoon, Mark R.

2009

MIMS EPrint: **2009.101**

Manchester Institute for Mathematical Sciences
School of Mathematics

The University of Manchester

Reports available from: http://eprints.maths.manchester.ac.uk/
And by contacting: The MIMS Secretary
School of Mathematics
The University of Manchester
Manchester, M13 9PL, UK

ISSN 1749-9097

Elongated S-cone stimuli reveals the importance of the intermediate temporal filter

Rigmor C. Baraas

Department of Optometry and Visual Science, Buskerud University College, 3611 Kongsberg, Norway

Janus J. Kulikowski

Faculty of Life Sciences, University of Manchester, Manchester M60 1QD, UK

Mark R. Muldoon

Faculty of Engineering and Physical Sciences, School of Mathematics, University of Manchester, Manchester M13 9PL, UK

The relative involvement of different temporal frequency-selective filters underlying detection of chromatic stimuli were studied. Diverse spectral stimuli were used, namely flashed blue and yellow light spots, wide bars and narrow bars. The stimuli were temporally modulated in luminance having constant wavelength. Although stimulus elongation apparently reduced the sensitivity at short and long wavelengths, the cone-opponent mechanism still remained responsible for the actual stimulus detection at different temporal frequencies. Stimulus elongation increased sensitivity for temporal frequencies around 3-6 Hz, revealing involvement of the intermediate temporal frequency-selective filters to detection, the so-called first *transient-1* filter. A probability summation model for the method of adjustment was developed that assumes that detection depends on the properties of the temporal filters underlying the temporal frequency-sensitivity curve. The model supports the notion that at least two temporal frequency-selective filters are necessary to account for the shape of the sensitivity curves obtained for blue stimuli.

OCIS codes: 330.1690, 330.1720, 330.6180, 330.6790, 330.5510

1. Introduction

It is now generally thought that three overlapping temporal frequency-selective filters subserve perception of achromatic stimuli [1–5]. These three temporal filters (or channels) can be revealed using a detection task combined with a task of identification of a stimulus, namely detection of pattern, movement and pure flicker [1,6] and corresponds to the three perceptual phenomena [7]. Mandler and Makous [2] also reported three achromatic temporal frequency filters: one low-pass, often referred to as *sustained* (actually weak band-pass, peak around 0.6-1 Hz), one intermediate band-pass referred to as *transient-1* (peak around 3-8 Hz), and a second band-pass referred to as *transient-2* (peak 9-16 Hz). The temporal frequencies at which the peaks occur depend on mean luminance, i.e. higher frequencies at higher luminance. The broad tuning of these filters makes it generally difficult to separate them, unless stimuli are chosen to favor certain components, or observers are made to perform discrimination tasks. The peak of the *transient-1* temporal filter is most readily revealed in luminance modulated elongated patterns such as gratings [6, 8]. Kelly [8], whilst not recognizing separate filters, observed that luminance modulation is sensitized for frequencies around 5 Hz, following introduction of a bipartite field (a central edge). He also reported that elongation of a chromatic stimulus lowered maximum sensitivity of the low-pass filter. Accordingly, two temporal filters for red-green elongated stimuli have been explicitly reported using Gabor patches [9, 10]; a low-pass filter (*sustained*), and a second band-pass filter (*transient-2*). There are strong residual achromatic contributions due to the L- and M-cone phase shifts

for red-green stimuli [11, 12], and this makes it more difficult to separate either of them from the luminance mechanism. Hence, the first or intermediate band-pass temporal filter (*transient-1*) has never been proposed as underlying detection of diffuse chromatic spots. The idea put forward here is that the presence of spatial edges is needed to reveal it. S-cone stimuli, like blue presented on a yellow adapting background, give better isolation of the cone-opponent mechanisms than L- and M-cone stimuli. Any evidence of involvement of temporal filters other than the low-pass (sustained) filter would then be taken as evidence for multiple temporal filters subserving chromatic perception in general.

The present study employed elongated stimuli like bars to investigate the number and type of temporal filters needed to account for detection of blue-yellow stimuli. This was done in an attempt to address the question whether the intermediate band-pass temporal frequency-selective filter (*transient-1*) is needed in addition to the low-pass temporal frequency-selective filter (*sustained*) to subserve chromatic processing in general. The addition of high-spatial frequency components, like edges, to S-cone stimuli still left the stimuli predominantly cone-opponent. Thresholds were measured as a function of temporal frequency for short (blue) and medium (yellow) wavelength and it is demonstrated that there is increased temporal sensitivity around 3-8 Hz for the S-cone isolated stimuli, suggesting involvement of the *transient-1* filter. A probability summation model was developed and fitted to the experimental data and shows that at least two temporal filters are needed to account for the results. That is: a low-pass filter (*sustained*), and an intermediate band-pass filter (*transient-1*), and in some cases a second band-pass filter (*transient-2*).

The intermediate temporal filter (*transient-1*) is considered to subserver perception of both color and luminance contrast, but color contrast, and not luminance contrast, is believed to be responsible for detection of blue stimuli for the following reasons:

i) Sensitivity to color contrast is much higher than that for luminance contrast in end-spectral regions.

ii) The intermediate temporal filter is also evident when the L- M cone-opponent mechanism has been additionally desensitized with an adapting yellow background.

2. Methods

The stimuli were generated by a three-filter Maxwellian view optical system. All stimulus parameters (spatio-temporal and chromatic) as well as observer responses were controlled and analyzed by a computer. The set-up has been described in detail elsewhere [13].

A. Stimuli and backgrounds

The test stimuli were circular spots (1 deg), wide (0.5 x 3.0 deg) or narrow bars (0.06 x 1.3 deg). The width of the bars subtending 0.06 and 0.5 deg approximates half a cycle of a grating of about 8 and 1 c/deg, respectively. The background of luminous intensity 1000 td was neutral daylight (x = 0.42, y = 0.42, equivalent to a color temperature (CT) of 3350 K), here referred to as white, or yellow (x = 0.51, y = 0.47, CT = 2520 K). The yellow background was obtained by adding a Lee industrial filter No.104 to the background field (x = 0.49, y = 0.49). The yellow background was used to desensitize the L-M cone-opponent

mechanisms, and to facilitate detection of luminance contrast around 575 nm [14, 15].

Calibration of stimuli and backgrounds have been described in detail elsewhere [16, 17].

B. Procedures

In each experiment, the observer used an analogue control button to adjust the intensity of the test object. The stimulus was flickering continuously while the observers were instructed to adjust the intensity until the flicker just ceased to be seen and then made one step up to yield the threshold [18]. Thus these are thresholds for seeing flicker, not any other aspect of a stimulus. Moreover, subjects were encouraged to look away every few seconds to avoid adaptation to flicker. The method is less time consuming [19] and has proven to be as good as the alternative forced choice method [16] for experienced observers. For slow (1, 2, 2.5, 3 and 5 Hz) temporal presentations the observer was instructed to set the threshold for detecting the offset of the test object (seeing the blank between presentations). For rapidly flickering (7.5, 10, 15 and 25 Hz) presentations, the observer was instructed to set the threshold for the detection of flicker [1,6], as during homochromatic flicker photometry [20]. In all experiments, the observer was first dark adapted for 20 min and then adapted to the background for a period of one min before the trials commenced. For spectral sensitivity measurements eleven wavelength presentations, from 400 to 650 nm was repeated at least three times. For temporal frequency measurements, three wavelengths (423 nm, 450 nm, 574 nm) was used. Fixation was maintained central throughout (assisted by a fixation spot).

Two different experiments were carried out. In the first experiment spectral sensitivity

curves were measured for 1-deg spots, wide and narrow bars. Measurements of the eleven different wavelength presentations, ranging from 400 to 650 nm were repeated at least three times. Temporal modulation was 1 or 25 Hz square-wave with an additive non-zero base. In the second experiment, temporal sensitivity measurements were carried out for three different wavelengths (423 nm, 450 nm, and 574 nm) with the 1-deg spots, wide and narrow bars. Measurements of the three wavelengths were repeated at least three times and in random order. Temporal modulation was 1, 2, 2.5, 3, 5, 7.5, 10, 15 and 25 Hz square-wave.

The data presented were obtained from three experienced observers: a 28-year-old female, a 33-year-old male and a 62-year-old male. All observers had corrected monocular visual acuity of 6/6 or better, normal color vision tested with the Farnsworth-Munsell 100 Hue test, and no known ocular or general pathology that could have affected the results.

3. Model

A. Probability summation for the method of adjustment

Following Metha and Mullen [9], it was sought to characterize the observers' sensitivity curves in terms of Watson's probability summation model [21] and various combinations of filters drawn from a family of filters originally proposed by Koenderink [22]. The main idea required to generalize the probability summation model to experiments employing the method of adjustment, rather than a two-alternative forced-choice design based on stimuli of fixed temporal duration, is explained briefly below. This is followed by models fitted to the actual data and results. Mathematical details appear in the Appendix, Section A.

B. The probability of recording a threshold at contrast level C

The main result in Section A is an expression, Eqn. (A9), for $P(C,\, \nu :\, \tau,\, \sigma,\, \beta,\, \boldsymbol{A})$, the probability that a stimulus with contrast C and flicker frequency ν will not be detected by a system of filters specified by parameters τ, σ (which characterize, respectively, the rise-time and temporal duration of the impulse response functions); Weibull parameter β and three filter amplitudes given by the vector $\boldsymbol{A} = (A_0,\, A_1,\, A_2)$. These scale, respectively, the output of a low-pass filter h_0 and two band-pass filters, h_1 and h_2 (see Table 1 and Section A for details).

A threshold at contrast level C was recorded if:

i) the stimulus is visible at contrast level C, but ...

ii) the stimulus is *not* visible at contrast level γC, where $\gamma = 10^{-\epsilon/10} < 1$ and ϵ (in dB), is the smallest step in contrast that the viewing system permits: here $\epsilon = 0.3$.

In light of this design, the probability of recording a detection threshold C for a stimulus with flicker frequency ν is the product

$$(1 - P(C,\, \nu :\, \tau,\, \sigma,\, \beta,\, \boldsymbol{A})) \times P(\gamma C,\, \nu :\, \tau,\, \sigma,\, \beta,\, \boldsymbol{A}) \tag{1}$$

where the first factor is the probability that the stimulus *is* detected at contrast C while the second is the probability that it is *not* detected at contrast γC.

C. *Bayesian model fitting*

The model builds upon Metha and Mullen's work in two ways, firstly by extending their models to encompass the method of adjustment and secondly by adopting a Bayesian framework for model fitting. The Bayesian approach requires the specification of a prior distribution $P(\tau,\, \sigma,\, \beta,\, \boldsymbol{A})$ on the parameters of the model, which should incorporate any *a priori* knowledge or assumptions about their values. Given the prior, parameters can be fit by choosing those that maximize the posterior likelihood, which is the product

$$P(\tau,\, \sigma,\, \beta,\, \boldsymbol{A}) \times P(\text{Data}\,|\,\tau,\, \sigma,\, \beta,\, \boldsymbol{A}) \tag{2}$$

In the remainder of this section a brief account of the factor $P(\text{Data}\,|\,\tau,\, \sigma,\, \beta,\, \boldsymbol{A})$ is given and the assumptions incorporated into the priors are explained.

1. *Likelihood of the data given parameters*

Data from a typical observer consists of several threshold measurements recorded at each of a range of frequencies: the data is denoted as a list of pairs $(C_{j,k},\, \nu_j)$ where ν_j ranges over the flicker frequencies at which there are data and, for each fixed value of j (that is, for each fixed flicker frequency), the index $k = 1,\, 2,\, \ldots$ runs over all the available threshold measurements. Given a set of parameters $(\tau,\, \sigma,\, \beta,\, \boldsymbol{A})$ the probability of a observing particular set of data is

$$P(\text{Data}\,|\,\tau,\, \sigma,\, \beta,\, \boldsymbol{A}) = \prod_{j,k} \left(1 - P(C_{j,k},\, \nu_j : \tau,\, \sigma,\, \beta,\, \boldsymbol{A})\right) P(\gamma C_{j,k},\, \nu_j : \tau,\, \sigma,\, \beta,\, \boldsymbol{A}). \tag{3}$$

This expression, when combined with prior distributions sketched below, enables us to fit the parameters by maximizing the posterior likelihood (2). C++ programs was written to do this, using version 3.1.1 of the discrete Fourier transform library FFTW [23] to compute convolutions (A4) and version 2.4 of Sandia's OPT++ library [24] to do the optimization.

2. The parameter β

Initial numerical investigations showed that for the data the conditional likelihood (3) depends only weakly on the parameter β. This makes sense in that β controls the slope of the psychometric function, but does not influence the threshold [21]. As only thresholds were measured, the data provide only weak constraints on β (though β does allow one to predict the variance for repeated threshold measurements at the same frequency). Metha and Mullen [9] addressed a similar issue by measuring the slope of the psychometric function directly, but such measurements were not available and so assumed fixed values of β were: 1.73 for the blue stimuli and 2.4 for yellow ones.

3. Priors on parameters of the filters

The shapes of Koenderink's family of kernels are characterized by only two parameters, τ and σ [see Eqn. (A3)], but a natural quantitative description of the three filters that are of interest here would require at least five: a roll-off frequency for the low-pass filter and two parameters apiece for each of the band-pass filters; for example, a frequency at peak gain and a full width at half-maximum. Thus Koenderink's formulation imposes certain inescapable interdependencies among the three filter. To incorporate the expectations about the filters

a prior distribution on τ and σ proportional to a product of normal distributions designed to constrain features of the gain curves was therefore applied.

The prior, which was the same far all classes of models, whichever combination of filters they included, was

$$P(\tau,\, \sigma,\, \beta,\, \boldsymbol{A}) = P(\tau,\, \sigma) = \prod_{j=0}^{2} \frac{e^{-(f_j(\tau,\sigma)-m_j)^2/(2s_j^2)}}{\sqrt{2\pi s_j^2}} \tag{4}$$

where the $f_j(\tau, \sigma)$ are frequencies at which certain features of the filters occur, the m_j are target values for those frequencies and the s_j are tolerances indicating how strictly the targets should be enforced. Thus, for example, $f_0(\tau, \sigma)$ is the frequency at which the low-pass filter rolls off to half-maximal gain and $m_0 = 8$ Hz while $s_0 = 3$ Hz. This component of the prior acts as a penalty function designed to provide a (fairly weak) constraint that requires the low-pass filter to roll off at $f_0 \approx 8 \pm 3Hz$. The other two factors in (4) are designed to constrain $f_1(\tau, \sigma)$ and $f_2(\tau, \sigma)$, which are the frequencies at which the two band-pass filters produce their peak gains. The details of these Gaussian priors are summarized in Table 1. Finally, uniform priors on the filters gains A_j were imposed, restricting each to the interval $0 \leq A_j \leq 25000$. Numerical experiments show that this range includes all remotely plausible (in terms of fitting the data) values.

(Table 1 about here)

4. Results

A. The 1 Hz spectral sensitivity function

Figure 1 shows the standard spectral sensitivity function of the cone-opponent mechanisms for two observers on the white background (3350 K), marked by empty circles. This curve has three characteristic, almost equal, peaks at about 450, 525 and 600-620 nm. A notch at 574 nm separates the peaks in the red-green spectral range (cf. Ref. 20,25,26) and conceals a response of the yellow-blue mechanism (cf. Ref. 13). The notch is defined as the difference in sensitivity at 574 nm as compared to at 554 nm and 601 nm. The notch becomes shallower when luminance intrusions are stronger (cf. Ref. 27). Fig. 1 illustrate this point: spectral sensitivity for a 1-deg spectral spot presented on the white background (empty circles) has a deeper notch than on the yellow background (2520 K), marked by filled circles.

(Figure 1 about here: one column width)

1. The effect of elongated stimuli on a common spectral sensitivity function

The spectral sensitivity curve obtained with the wide bar on a white background (Fig. 1: empty squares) is only marginally different to that obtained with a 1-deg spot (empty circles), especially for medium-long wavelengths. The notch depth (cf. Ref. 27) at 574 nm is reduced by about 0.1 log units as compared to the spot, whereas the peak around 450 nm is reduced by about 0.05 log units.

Narrowing the bar to 0.06 deg (Fig. 1: empty triangles) reduced sensitivity at 450 nm by 0.6 to 1.0 log unit depending on the observer. The short-wavelength peak is reduced by

about 0.3 log units compared to the spot. Thus the sensitivity of the short-wavelength cone-opponent mechanism seems to deteriorate as a consequence of elongation of the stimuli when a white background is used. There is still a difference between cone-opponent and luminance mechanisms in end-spectral regions, even for the narrow bar: Compare empty triangles with the dashed line in Fig. 1; the dashed line represents 25 Hz homochromatic flicker for a narrow bar on a white background. The 25 Hz homochromatic flicker function is identical for the yellow background and is therefore not shown here.

2. The effect of elongated stimuli and background color

A yellow background was introduced to desensitize the L- and M-cone mechanisms (Fig. 1, filled circles). Spectral sensitivity curves measured for bars, either wide or narrow, presented on the yellow background are enhanced for the short-wavelength range as compared with the curves obtained for the white background. Similar effects, which have been known for spot stimuli (Fig. 1, circles), is evident for narrow and wide bars as well (compare filled squares and triangles with the corresponding empty symbols in Fig. 1), indicating isolation of the S-cone opponent mechanism. The shallower notch around 574 nm may imply that the detection of spectral yellow in this case is influenced by luminance contrast, since the test and background differ little in chromaticity.

B. The temporal sensitivity function

1. The effect of elongated stimuli and background color

(Figure 2 (double column width) about here).

Actual thresholds and predicted sensitivity curves for spots are plotted in Fig. 2 and for wide and narrow bars in Fig. 3, 4, 5. The temporal frequency sensitivity curves obtained with a 2-deg coloured spot on a white background generally gives a low-pass function (cf. Ref. 28). This is similar to what is presented here for a 1-deg blue spot on a yellow background [Fig. 2(b)]. A blue wide bar gives rise to a broader low-pass function with a flat region between 3 to 10 Hz [Figs. 3 (a) and 4 (a)]. The flat region of the function may be an envelope of the sensitivities of two band-pass (transient) filters.

(Figures 3 (double column width), 4,(double column width), 5 (double column width) about here).

Tables 2-6 summarize the results from the model fit. The tables have the same format: the likelihood scores for a given stimulus are arranged in a block of four rows; one each for the four classes of model that were tested. Each row begins with a symbol describing the model, for example, M_{02} refers to a model based on the low-pass filter h_0 and the band-pass filter h_2, followed by three columns relating to the log of the posterior-likelihood for the maximally likely set of parameters. The column headed *Prior* lists the log of the Bayesian prior (4) evaluated for the parameters of the most likely model while the column headed *Fit* is the log of that factor (3) in the posterior likelihood (2) which gives the probability of seeing the

observed data: the latter of these two provides a measure of how well the most likely model in the class actually fits the data. The last column of log-likelihood values, headed *Total*, gives the sum of the contributions from the prior and the fit and it is this quantity, the log of the posterior likelihood (2), that is the target of the likelihood maximization.

The final two columns list p-values given by a test of the significance of the differences in log-likelihood between the various models. The test depends on an asymptotic result for the distribution of these differences that requires the models being compared to be are *nested* in the sense that one is a special case of the other. Consider, for example, the models M_0 and M_{02}: the first includes only a single filter, the low-pass filter h_0, while the second includes both h_0 and h_2, the second of the band-pass filters. Thus M_0 is a special case of M_{02} for which the amplitude $A_2 = 0$. In the vocabulary of the asymptotic result mentioned above, model M_0 is said to be nested in model M_{02} and a χ^2 test can be used (see, for example, Section 8.4.2 of Ref. 29) to check whether the difference in log-likelihood between the two models is significant. This makes it clear that there are two sorts of significance tests that can be done. As M_0 is nested within each of the more complex models, it is possible to test all three of them against M_0: the p-values for these tests are tabulated in the columns headed p_1. The same framework to test differences in likelihood between models M_{01} and M_{02} can not be used as neither is nested within the other, but both of these two can be tested against the model M_{012}. The columns headed p_2 record p-values for the difference in log-likelihood between M_{012} and the most likely member of the pair M_{01} and M_{02}.

(Table 2, 3 and 4 about here).

Tables 2 and 3, top two rows, show that in the case of a blue bar on a white background, a model that combines the low-pass filter with the first band-pass filter (model class M_{01}), or a model that combines all three filters (model class M_{012}) provides the best fit to the data. The model that excludes the first band-pass filter and combines the low-pass filter with the second band-pass filter (model class M_{02}) provides the least satisfactory fit to the data. For a narrow blue bar the model M_{012} has a slightly greater likelihood than either M_{01} or M_{02}, but the difference is not significant.

2. The effect of elongated stimuli and background color

The predicted temporal-sensitivity curves for a blue wide bar on a yellow background [Figs. 3(c), 4(c), and 5(a)] are similar to those for a blue wide bar on a white background [Figs. 3(a) and 4(a)], this is confirmed in the log-likelihood values for each of the model fits (tables 2, and 3). Table 4 show the result for observer AG for a blue spot and wide and narrow blue bars on a yellow background; his results show the same trend. This indicates that a *transient-1* filter also subserves detection of S-cone stimuli. Narrowing the bar shifts the peak of the predicted sensitivity curves to lower temporal frequencies, as a wide bar, detected by its two edges, is known to engage faster processing than a narrow bar (cf. Ref. 30). Hence, the detection of the stimulus depend on stimulus shape as well as stimulus color at intermediate temporal frequencies, utilising both information about chromatic and luminance contrast.

A yellow bar, wide or narrow, on a yellow background gives rise to a temporal sensitivity curve with a peak around 10 Hz [Figs. 3(e) and (f) and 4(e) and (f)]. Tables 5 and 6 show that the model that fits a yellow spot or bar best is either the model that combines the low-pass filter with the second band-pass filter (model class M_{02}), or a model that combines all three filters (model class M_{012}). The model that combines the low-pass filter with the first band- pass filter (model class M_{01}) provides the poorest fit to the data.

(Table 5 and 6 about here).

5. Discussion

The results show that at least two temporal frequency-selective filters (or channels) are necessary to account for detection of both chromatic (blue bars on a yellow or a white background) and achromatic (yellow bars on a yellow background) stimuli. The second *transient-2* filter, however, dominates the predicted sensitivity curves obtained with the yellow bar, whereas the first *transient-1* filter is the transient filter that dominates the predicted sensitivity curves obtained with the blue bar. This transition reveals a shift in relative contributions of color and luminance from low to higher temporal frequencies, and we argue that interaction between color and luminance signals drives visual processing at intermediate temporal frequencies.

The deterioration of the cone-opponent function as a consequence of change of shape from a spot to a bar can be inferred from the change in the spectral sensitivity functions (Fig. 1). One plausible explanation for the observation is that elongated stimuli (presented at 1 Hz)

activate a hypothetical intermediate detection mechanism operating between pure color, mediated by the *sustained* temporal filter, and pure luminance, mediated by the *transient-2* temporal filter. This is not an effect of area since the change in effective area of a spot, from 0.1 deg^2 to above 1 deg^2, only produces a vertical shift in sensitivity [19]. Note that pattern-detection sensitivity is known to increase when straight edges are present in the stimuli [31], unlike pure luminance detection, which is best for large spots [1].

The presence of straight edges in the stimuli still increases the activation of the luminance mechanism as compared with the cone-opponent mechanism, and this is evident in the spectral sensitivity function as the notch around 575 nm is shallower and end-spectral sensitivity at 450 and 600 nm is reduced for the bar stimuli as compared with the spot stimulus (Fig. 1). These results are in line with previous quantitative assessments of contribution of cone-opponent versus luminance mechanism around 575 nm [13, 20, 32–37]. Reviewing the experimental evidence available, Sharanjeet-Kaur et al. [27] concluded that circular blurred spots, or spots with an annulus, are optimal stimuli to activate cone-opponent mechanisms. Introduction of a yellow background further increases chance achromatic detection [13, 15], and makes it is difficult to isolate the yellow chromatic part of the blue-yellow cone-opponent mechanism, especially if the wavelengths of the test stimulus and background are similar [13]. Conversely, the yellow background accentuates chromatic detection for a stimulus with peak wavelength around 450 nm as a consequence of L- and M-cone desensitizing. Luminance contrast is thereby unlikely to be responsible for detection at 450 nm, and thus the results for blue stimuli suggest different processes.

Stimuli with straight edges like the bar stimuli employed here are not optimal shapes for stimulation of the cone-opponent mechanisms as elongation of spots reduces the peaks at both ends of the visible spectrum as shown previously [38]. Narrowing the bars reduces the spectral sensitivity of the peak around 450 nm even more, probably because of foveal tritanopia [39,40]. Apparently, even though the sensitivity of the cone-opponent mechanism to elongated stimuli is lower than for spots, the sensitivity of the luminance mechanism under such viewing conditions is even lower (see Fig. 1 dashed line the 25 Hz homochromatic flicker function approximates the luminosity function). The luminance mechanism does not contribute much in the spectral sensitivity function at both ends of the visible spectrum. Detection of blue bars is thus mediated mainly by the cone-opponent mechanism. Furthermore, measurements performed on yellow backgrounds, show an overall increase of sensitivity around 450 nm, indicating isolation of the S-cone response.

In spite of the quantitative differences in the spectral sensitivity curves for the various conditions of detection of narrow and wide blue bars, the predicted temporal sensitivity curves reveal the presence of the same intermediate (*transient-1*) filter for blue bars on white and yellow backgrounds. Moreover, the models that include the *transient-1* filter also provides the best fit to the data (e.g. Table 2).

A. The temporal sensitivity function

The detection of a blue spot on a white background by cone-opponent mechanism is well isolated from the luminance mechanism, as defined by homochromatic flicker photometry.

The temporal frequency curve under this condition is low-pass with a fall-off at 10 Hz [28, 41]. The predicted sensitivity curves obtained for a blue bar with both white and yellow background conditions are flat between 3 and 10 Hz with lower sensitivity at low temporal frequencies [Figs. 3 and 4 (a) and (b)] than for a 1-deg spot stimulus [compare Fig. 2 (b) with Figs. 3 (c), 4 (c) and 5 (a)]. The flattening at intermediate frequencies of the temporal sensitivity curves reflects that under conditions were spatial edges are prominent, the cone-opponent mechanism, which is believed to be of sustained properties only, is not operating on its own. The argument put forward here is that this is because perception is mediated by the first *transient-1* filter. The model employed to derive the theoretical filters underlying the data support that at least two filters are necessary to account for the data, with models encompassing both the *sustained* and the *transient-1* filters being favoured. A similar effect was demonstrated with different intensity levels of the yellow background [42], giving a flatter region between 4 and 9 Hz at lower levels of background illumination. Stockman *et al.* also reported that S- cone signals are mediated by two temporal filters [43]; the *sustained* and the *transient-2* filters. They used high intensity levels that shift sensitivity to higher temporal frequencies; this may be why they did not consider the *transient-1* filter. Any contribution of the first *transient-1* filter has been shown to be evident if the temporal frequency sensitivity curve exhibits a peak around 4 Hz [6, 44]. Involvement of a distinctive intermediate transient component has been reported for red-green isoluminant stimuli and has been attributed to the operation of an additional chromatic mechanism [10, 45]. It has been demonstrated by two other separate investigations [46, 47] that under strict conditions of isoluminance, and

after accounting for this transient component, that both red-green and blue-yellow (tritan) cone-opponent mechanisms are purely low-pass at threshold. This implies that the cone-opponent mechanism cannot be the sole operator over the range of intermediate temporal frequencies.

1. Related studies

The three temporal frequency-selective filters apparent in the data presented here are most likely to represent the following: a *tsustained* filter subserving perception of pure color (or cone-opponent), one *transient-1* filter of mixed color and luminance properties, and a second *transient-2* filter of pure luminance properties. While retrospectively analyzing early studies it became apparent that the intermediate *transient-1* filter was actually evident in the data of Robson [48] (counter-phased luminance gratings) and Kelly [8] (a bipartite field). Kulikowski and Tolhurst [6] revealed two different temporal frequency-selective filters for oriented achromatic stimuli. Furthermore, two discrete temporal frequency-selective filters were reported for detecting chromatic and oriented stimuli [42] and straight-line contours [49]. Finally, a similar finding has been reported in S-cone monochromatic observers [50].

The slow low-pass (sustained) filter was identified as exclusively serving fine pattern detection above 25 c/deg [51]. A similar filter is also serving the detection of color as reviewed recently [46,47]. On the other hand, the *transient-1* filter, responsible for motion perception, is stronger for elongated patterns, and is clearly separable from pure flicker detection [1]. The so-called movement mechanism, optimal around 3-7 Hz and 2 c/deg, depending on level of

retinal illumination, may not have any contribution from the second *transient-2* filter (pure flicker mechanism). Burr and Ross [44] have shown that most spatio-temporal contributions to the detection of fast motion are due to a transient filter with peak sensitivity around 4 Hz (the first *transient-1* filter). The predominance of the second *transient-2* filter over the first *transient-1* filter is shown only above 25 Hz for flashed spots [41].

2. Chromatic pattern mechanism: possible neuronal basis

S-, M- and L-cones make characteristic connections in the retina via bipolar neurons (for review see: [52]). S-cones do not project to magnocellular ganglion neurons. Dacey and Lee [53] have shown that excitatory S-cone input goes via specific bipolar neurons to distinct bistratified ganglion neurons and the koniocellular pathway [54] there from. S-cone inhibitory connections are associated with different neurons [55, 56]. Most numerous are L-M opponent connections forming the parvocellular pathway [57, 58]. In spite of these morphological differences, the +S-(L), +S-(M) and L-M opponent ganglion and LGN neurons have temporal characteristics that are not substantially different [56], and all exceed psychophysical limits of temporal resolution [59]. It is argued that the perceptual limits of temporal resolution must be determined at the cortical level [60]. Magnocellular neurons receive information as a non-linear sum from L+M cones; their spectral characteristics fit the V-lambda luminosity function best and are often regarded as substrate of luminance information [61–63]; but see [64] for an alternative view. Although it was argued that neurons that receive parvocellular input responds in a way that can approximate the V-lambda luminosity function [65],

both parvo- and koniocellular neurons have been reported to have too low luminance contrast sensitivity [56, 66–68] to contribute on their own to luminance contrast detection. Studies of single neurons in the monkey primary cortex V1, have revealed distinct color neurons that were not sensitive to luminance contrast [69–71], but in addition also many neurons that were sensitive to both color and luminance contrast. The latter are typically neurons with elongated receptive fields [72–78]. Mixing of parvo-, konio- and magnocellular pathways have been demonstrated anatomically in area V1 [68,79,80]. Moreover, neruons that received mixed input from the three pre-cortical pathways had the highest maximum achromatic contrast sensitivity at low spatial frequencies and moderate velocities. These composite neurons may form the basis of a mechanism that combines information of color, form and motion.

Kulikowski and Walsh [81, 82] introduced a concept of a chromatic-pattern, motion and stereo detection mechanism, which may process a mixture of color and luminance signals, possibly reflecting an integration of konio-, parvo- and magnocellular inputs. Its spectral characteristic depends critically on the shape of the stimulus; for a 1-deg spot it is the envelope of typical cone-opponent functions [20, 83]; for elongated stimuli, it is a weighted characteristic of the V-lambda luminosity function and the two cone-opponent mechanisms: red-green and blue-yellow.

This view is consistent with the finding of Metha and Mullen [10], who examined red-green isoluminant and luminance modulated Gabor patches involved in temporal frequency discrimination. They concluded that at least two temporal filters must be involved which correspond to the *sustained* and the *transient-1* filter. They suggested that the *transient-1*

filter might be part of the color detection process. However, McKeefry [46] argued that when the *transient-1* filter is excluded in an aberration-free experiment, red-green and blue-yellow sensitivity become equal and color is processed in a veridical manner. This would suggest separate systems for color and chromatic pattern analyzis, the latter would depend on the shape of the visual stimuli.

6. Conclusion

The data presented here demonstrate the involvement of the first *transient-1* filter in a task requiring the detection of elongated patterns with combined color and luminance contrast. Detection of spectral spots is predominantly executed by the cone-opponent mechanism (a *sustained* filter) at low temporal frequencies, and by the pure flicker (luminance) mechanism (the second *transient-2* filter) at very high temporal frequencies. The involvement of the *transient-1* filter for detecting elongated stimuli suggests that this temporal frequency-selective filter is linked with analyzis of chromatic patterns, integrating color and form in to a unified percept (cf. Ref. 84). It is postulated that this intermediate mechanism which is based on mixed konio-, parvo- and magnocellular input to some orientation sensitive visual cortical units [68] affect perception. The change of stimulus shape may critically alter the involvement of these units.

References

1. P. E. King-Smith and J. J. Kulikowski, "Pattern and flicker detection analysed by subthreshold summation," Journal of Physiology **249**(3), 519–548 (1975).
2. M. B. Mandler and W. Makous, "A three channel model of temporal frequency perception," Vision Research **24**(12), 1881–1887 (1984).
3. S. J. Anderson and D. C. Burr, "Spatial and temporal selectivity of the human motion detection system," Vision Research **25**(8), 1147–1154 (1985).
4. R. F. Hess and G. T. Plant, "Temporal frequency discrimination in human vision: Evidence for an additional mechanism in the low spatial and high temporal frequency region," Vision Research **25**(10), 1493–1500 (1985).
5. R. F. Hess and R. J. Snowden, "Temporal properties of human visual filters: number, shapes and spatial covariation," Vision Research **32**(1), 47–59 (1992).
6. J. J. Kulikowski and D. J. Tolhurst, "Psychophysical evidence for sustained and transient detectors in human vision," Journal of Physiology **232**(1), 149–162 (1973).
7. J. J. Kulikowski, "Some stimulus parameters affecting spatial and temporal resolution of human vision," Vision Research **11**(1), 83–93 (1971).
8. D. H. Kelly, "Luminous and chromatic flicker pattern have opposite effects," Science **188**, 371–372 (1975).
9. A. B. Metha and K. T. Mullen, "Temporal mechanisms underlying flicker detection and identification for red-green and achromatic stimuli," Journal of the Optical Society of

America A **13**(10), 1969–1980 (1996).

10. A. B. Metha and K. T. Mullen, "Red-green and achromatic temporal filters: a ratio model predicts contrast-dependent speed perception," Journal of the Optical Society of America A **14**(5), 984–996 (1997).
11. C. F. S. III, R. E. Kronauer, A. Ryu, A. Chaparro, and R. T. E. Jr., "Contributions of human long-wave and middle-wave cones to motion detection," Journal of Physiology **485**(1), 221–243 (1995).
12. C. F. S. III, A. Chaparro, A. S. Tolias, and R. E. Kronauer, "Colour adaptation modifies the long-wave versus middle-wave cone weights and temporal phases in human luminance (but not red-green) mechanism," Journal of Physiology **449**(1), 227–254 (1997).
13. Sharanjeet-Kaur, J. J. Kulikowski, and V. Walsh, "The detection and discrimination of categorical yellow," Ophthalmic and Physiological Optics **17**(1), 32–37 (1997).
14. M. Marré, "The investigation of acquired colour vision deficiencies," in *Colour*, pp. 99–135 (Adam Hilger, London, 1973).
15. A. Nacer, I. J. Murray, and J. J. Kulikowski, "Balancing sensitivity of human chromatic opponent mechanisms by adaptation," Journal of Physiology **P21**, 485P (1995).
16. K. T. Mullen and J. J. Kulikowski, "Wavelength discrimination at detection threshold," Journal of the Optical Society of America A **7**(4), 733–742 (1990).
17. G. Westheimer, "The Maxwellian view," Vision Research **6**, 669–682 (1966).
18. F. W. Campbell and J. J. Kulikowski, "Orientational selectivity of the human visual

system," Journal of Physiology **187**(2), 437–445 (1966).

19. A. Nacer, "The interaction between chromatic and achromatic mechanisms of human colour vision: Limitations of sensitivity," Ph.D. thesis, Department of Optometry and Vision Sciences, UMIST, Manchester, UK (1990).

20. P. E. King-Smith and D. Carden, "Luminance and opponent-colour contributions to visual detection and adaptation and to temporal and spatial integration," Journal of the Optical Society of America **66**, 709–717 (1976).

21. A. B. Watson, "Probability summation over time," Vision Research **19**(5), 515–522 (1979).

22. J. J. Koenderink, "Scale-Time," Biological Cybernetics **58**(3), 159–162 (1988).

23. M. Frigo and S. G. Johnson, "The Design and Implementation of FFTW3," Proceedings of the IEEE **93**(2), 216–231 (2005). URL `http://www.fftw.org/`.

24. J. Meza, R. Oliva, P. Hough, and P. Williams, "OPT++: An Object Oriented Toolkit for Nonlinear Optimization," ACM Transactions on Mathematical Software **33**(2), Article No. 12 (2007). URL `http://doi.acm.org/10.1145/1236463.1236467`.

25. H. G. Sperling and R. S. Harwerth, "Red-green cone interactions in the increment threshold spectral sensitivity of primates," Science **172**, 180–184 (1971).

26. D. H. Foster and R. S. Snelgar, "Test and field spectral sensitivities of colour mechanisms obtained on small white backgrounds: action of unitary opponent-colour processes," Vision Research **23**(8), 787–797 (1983).

27. Sharanjeet-Kaur, J. J. Kulikowski, and D. Carden, "Isolation of chromatic and achromatic mechanisms: a new approach," Ophthalmic and Physiological Optics **18**(1), 49–56 (1998).

28. H. D. Lange, "Research into the dynamic nature of the human fovea-cortex systems with intermittent and modulated light. I. Attenuation characteristics with white and coloured light," Journal of the Optical Society of America **48**, 777–784 (1958).

29. W. J. Ewens and G. R. Grant, *Statistical Methods in Bioinformatics: An Introduction* (Springer Verlag, New York, 2001).

30. P. E. King-Smith and J. J. Kulikowski, "Line, edge and grating detectors in human vision," Journal of Physiology **230**(1), 23P–25P (1973).

31. J. Bacon and P. E. King-Smith, "The detection of line segments," Perception **6**(2), 125–131 (1977).

32. C. R. I. Jr. and B. A. Drum, "How neural adaptation changes chromaticity coordinates," Journal of the Optical Society of America **63**(3), 369–373 (1973).

33. C. R. I. Jr. and E. Martinez, "Tonic-phasic-channel dichotomy and Crozier's law," Journal of the Optical Society of America **73**(2), 183–189 (1983).

34. J. J. Kulikowski and K. Kranda, "Detection of coarse patterns with minimum contribution from rods," Vision Research **17**(5), 653–656 (1977).

35. J. E. Thornton and E. N. Pugh, Jr., "Red/green colour opponency at detection threshold," Science **219**, 191–193 (1983).

36. R. S. Snelgar, D. H. Foster, and M. O. Scase, "Isolation of opponent-colour mechanisms at increment threshold," Vision Research **27**(6), 1017–1027 (1987).

37. D. J. Calkins, J. E. Thornton, and E. N. Pugh, Jr., "Monochromatism determined at a long-wavelength/middle-wavelength cone-antagonistic locus," Vision Research **32**(12), 2349–2367 (1992). Published erratum appears in Vision Res. 1993;33(8):1151.

38. R. C. Baraas, J. J. Kulikowski, and A. R. Robson, "Spatial edges reduce colour selectivity," Perception **27S**, 168–169 (1998).

39. D. R. Williams, D. I. MacLeod, and M. M. Hayhoe, "Punctate sensitivity of the blue-sensitive mechanism," Vision Research **21**(9), 1357–1375 (1981).

40. D. R. Williams, D. I. A. MacLeod, and M. M. Hayhoe, "Foveal tritanopia," Vision Research **21**, 1341–1356 (1981).

41. A. Nacer, I. J. Murray, Sharanjeet-Kaur, and J. J. Kulikowski, "Selectivity limits of spectral sensitivity functions for chromatic and achromatic mechanisms," in *John Dalton's Colour Vision Legacy*, pp. 83–91 (Taylor & Francis Ltd., London, 1997).

42. J. J. Wisowaty and R. M. Boynton, "Temporal modulation sensitivity of the blue mechanism: measurements made without chromatic adaptation," Vision Research **20**(11), 895–909 (1980).

43. A. Stockman, D. I. MacLeod, and D. D. DePriest, "The temporal properties of the human short-wave photoreceptors and their associated pathways." Vision Res **31**(2), 189–208 (1991).

44. D. C. Burr and J. Ross, "Contrast sensitivity at high velocities," Vision Research **22**, 479–484 (1982).

45. D. J. McKeefry and J. J. Kulikowski, "Spatial and temporal sensitivities of colour discrimination mechanisms," in *John Dalton's Colour Vision Legacy*, pp. 163–172 (Taylor & Francis Ltd., London, 1997).

46. D. M. McKeefry, I. J. Murray, and J. J. Kulikowski, "Red-green and blue-yellow mechanisms are matched in sensitivity for temporal and spatial modulation," Vision Research **41**, 245–255 (2001).

47. A. G. Shapiro, L. A. Baldwin, and J. D. Mollon, "The S and L-M chromatic system have matched temporal processing characteristics only at low-light levels," Perception **31**, S68b (2002).

48. J. G. Robson, "patial and temporal contrast sensitivity of the human eye," Journal of the Optical Society of America **56**, 1141–1150 (1966).

49. P. Cavanagh, D. I. A. MacLeod, and S. M. Anstis, "Equiluminance: spatial and temporal factors and the contribution of blue-sensitive cones," Journal of the Optical Society of America A **4**(8), 1428–1438 (1987).

50. R. F. Hess, K. T. Mullen, and E. Zrenner, "Human photopic vision with only short wavelength cones: post-receptoral properties," Journal of Physiology **417**, 151–172 (1989).

51. M. H. Russell, J. J. Kulikowski, and I. J. Murray, "Spatial frequency dependence of the human visual evoked potential," in *Evoked Potentials III*, pp. 231–239 (Butterworth,

Baltimore, 1987).

52. P. R. Martin, "Colour processing in the primate retina: recent progress," Journal of Physiology **513**, 631–638 (1998).

53. D. M. Dacey and B. B. Lee, "The 'blue-on' opponent pathway in primate retina originates from a distinct bistratified ganglion cell type," Nature **367**, 731–735 (1994).

54. P. R. Martin, A. J. R. White, A. K. Goodchild, H. D. Wilder, and A. E. Sefton, "Evidence that blue-on cells are part of the third geniculocortical pathway in primates," European Journal of Neuroscience **9**(7), 1536–1541 (1997).

55. D. J. Calkins, "Representation of cone signals in the primate retina," Journal of the Optical Society of America A **17**(3), 597–606 (2000).

56. C. Taliby, S. G. Solomon, and P. Lennie, "Functional asymmetries in visual pathways carying S-cone signals in Macaque," Journal of Neuroscience **28**(15), 4078–4087 (2008).

57. M. S. Livingstone and D. H. Hubel, "Anatomy and physiology of a color system in the primate visual cortex," Journal of Neuroscience **4**(1), 309–356 (1984).

58. D. Y. Ts'o and C. D. Gilbert, "The organization of chromatic and spatial interactions in the primate striate cortex," Journal of Neuroscience **8**, 1712–1728 (1988).

59. T. Yeh, B. B. Lee, and J. Kremers, "Temporal response of ganglion cells of the macaque retina to cone-specific modulation," Journal of the Optical Society of America A **12**(3), 456–464 (1995).

60. J. Cass, C. W. G. Clifford, D. Alais, and B. Spehar, "Temporal structure of chromatic

channels revealed through masking," Journal of Vision **9(5)**(17), 1–15 (2009).

61. B. B. Lee, P. R. Martin, and A. Valberg, "Nonlinear summation of M- and L-cone inputs to phasic retinal ganglion cells of the macaque," Journal of Neuroscience **9**(4), 1433–1442 (1989).

62. B. B. Lee, J. Pokorny, V. C. Smith, P. R. Martin, and A. Valberg, "Luminance and chromatic modulation sensitivity of macaque ganglion cells and human observers," Journal of the Optical Society of America A **7**(12), 2223–2236 (1990).

63. P. Lennie, J. Pokorny, and V. C. Smith, "Luminance," Journal of the Optical Society of America A **10**(6), 1283–1293 (1993).

64. W. H. Merigan and J. H. Maunsell, "Macaque vision after magnocellular lateral geniculate lesions." Vis Neurosci **5**(4), 347–352 (1990 Oct).

65. P. Gouras and E. Zrenner, "Enchancement of luminance flicker by color-opponent mechanisms," Science **205**, 587–589 (1979).

66. E. Kaplan and R. M. Shapley, "X and Y cells in the lateral geniculate nucleus of the macaque monkeys," Journal of Physiology **330**, 125–143 (1982).

67. T. P. Hicks, B. B. Lee, , and T. R. Vidyasagar, "The responses of cells in macaque lateral geniculate nucleus to sinusoidal gratings," Journal of Physiology **337**, 183–200 (1983).

68. T. R. Vidyasagar, J. J. Kulikowski, D. M. Lipnicki, and B. Dreher, "Convergence of parvocellular and magnocellular information channels in the primary visual cortex of the macaque," European Journal of Neuroscience **16**(5), 945–956 (2002).

69. T. Yoshioka and B. M. Dow, "Colour, orientation and cytochrome oxidase reactivity in areas V1, V2 and V4 of macaque monkey visual cortex," Behavioural Brain Research **76**(1-2), 71–88 (1996).

70. T. Yoshioka, B. M. Dow, and R. G. Vautin, "Neuronal mechanisms of colour categorization in areas V1, V2 and V4 of macaque monkey visual cortex," Behavioural Brain Research **76**(1-2), 51–70 (1996).

71. J. J. Kulikowski and V. Walsh, "Colour vision: isolating mechanisms in overlapping streams," Progress in Brain Research **95**, 417–426 (1993).

72. C. R. Michael, "Color-sensitive complex cells in monkey striate cortex," Journal of Neurophysiology **41**(5), 1250–1266 (1978).

73. C. R. Michael, "Color vision mechanisms in monkey striate cortex: simple cells with dual opponent-color receptive fields," Journal of Neurophysiology **41**(5), 1233–1249 (1978).

74. R. G. Vautin and B. M. Dow, "Color cell groups in foveal striate cortex of the behaving macaque," Journal of Neurophysiology **54**(2), 273–292 (1985).

75. R. L. D. Valois and K. K. D. Valois, "Neural coding of colour," in *Handbook of Perception*, vol. 5, pp. 117–166 (Academic Press, New York, 1975).

76. R. L. D. Valois and K. K. D. Valois, "A multi-stage color model," Vision Research **33**(8), 1053–1065 (1993).

77. P. Lennie, J. Krauskopf, and G. Sclar, "Chromatic mechanisms in striate cortex of macaque," Journal of Neuroscience **10**(2), 649–669 (1990).

78. E. N. Johnson, M. J. Hawken, and R. Shapley, "The spatial transformation of color in the primary visual cortex of the macaque monkey," Nature Neuroscience **4**(4), 409–416 (2001).

79. J. S. Lund, Q. Wu, P. T. Hadingham, and J. B. Levitt, "Cells and circuits contributing to functional properties in area V1 of macaque monkey cerebral cortex: bases of neuroanatomically realistic models," Journal of Anatomy **187**, 563–581 (1995).

80. T. R. Vidyasagar, J. J. Kulikowski, A. Robson, and B. Dreher, "Responses of V1 cells in primate reveal excitatory convergence of P and M channels," European Journal of Neuroscience **10**, S239 (1998).

81. J. J. Kulikowski and V. Walsh, "Demonstration of binocular fusion of color and texture," in *Early Vision and Beyond*, T. Papathomas, ed., pp. 27–32 (MIT Press, Cambridge, Massachusetts, 1995).

82. J. J. Kulikowski, "Spatial and temporal properties of chromatic processing: Separation of colour from chromatic pattern mechanisms," in *John Dalton's Colour Vision Legacy*, pp. 133–146 (Taylor & Francis Ltd., London, 1997).

83. K. Kranda and P. E. King-Smith, "What can colour thresholds tell us about the nature of the underlying detection mechanisms," Ophthalmic and Physiological Optics **4**(1), 83–87 (1984).

84. C. W. G. Clifford, B. Spehar, S. G. Solomon, P. R. Martin, and Q. Zaidi, "Interactions between color and luminance in the perception of orientation." J Vis **3**(2), 106–115

(2003).

A. Probability summation model for the method of adjustment: mathematical details

Watson's probability summation model [21] requires two ingredients: a set of filters and a probabilistic detection model. For the first, we followed Metha and Mullen [9] and built models based on combinations of three filters—a low-pass filter and two band-pass filters—whose impulse response functions are

$$h_0(t\,:\,\tau,\,\sigma) = \exp\left\{-\frac{(\ln(t/\tau))^2}{\sigma^2}\right\} \tag{A1}$$

$$\begin{aligned} h_1(t\,:\,\tau,\,\sigma) &= dh_0/dt \\ &= -\left(\frac{2}{t\sigma^2}\right)\ln(t/\tau)\exp\left\{-\frac{(\ln(t/\tau))^2}{\sigma^2}\right\} \\ &= -\left(\frac{2}{t\sigma^2}\right)\ln(t/\tau)h_0(t) \end{aligned} \tag{A2}$$

$$\begin{aligned} h_2(t\,:\,\tau,\,\sigma) &= dh_1/dt \\ &= -\left(\frac{2}{t^2\sigma^4}\right)\left[\frac{2}{\sigma^4}\ln(t/\tau)^2+\ln(t/\tau)-1\right]\exp\left\{-\frac{(\ln(t/\tau))^2}{\sigma^2}\right\} \\ &= -\left(\frac{2}{t^2\sigma^2}\right)\left[\frac{2}{\sigma^2}(\ln(t/\tau))^2+\ln(t/\tau)-1\right]h_0(t). \end{aligned} \tag{A3}$$

Here the parameters τ and σ characterize, respectively, the rise-times and temporal durations of responses.

If the stimulus flickers periodically with contrast C, frequency ν (in Hz.) and temporal waveform $g(t:\nu)$ then the responses of the various filters are given by convolutions:

$$\begin{aligned} R_j(t) &= Cg(t\,:\,\nu) * h_j(t\,:\,\tau,\,\sigma) \\ &= C\int_0^\infty g(t-s:\,\nu)h_j(s\,:\,\tau,\,\sigma)\,ds \end{aligned} \tag{A4}$$

where, on the left-hand side, the dependence on the parameters τ and σ has been suppressed. Note that as the waveforms $g(t:\nu)$ are periodic with period $1/\nu$, so are the responses $R_j(t)$. In terms of the $R_j(t)$, the probability that a subject would *fail* to detect the stimulus during some interval $T_0 \le t \le T_1$ is given by

$$P_W(C, \nu: \tau, \sigma, \beta, \boldsymbol{A}) = 2^{-\int_{T_0}^{T_1} \sum_{j=0}^{2} |A_j R_j(t)|^\beta \, dt} \tag{A5}$$

where here the dependence on all parameters is shown explicitly, including the vector of amplitudes $\boldsymbol{A} = (A_0, A_1, A_2)$ and the Weibull parameter β that comes from Watson's probabilistic detection model.

Application of (A5) is straightforward when the signal is presented for a finite period (thus fixing the bounds T_0 and T_1 of the integral), but has no immediately obvious interpretation when, as in our experiments, the flickering stimulus is presented essentially continuously, with the subject deciding whether the stimulus is visible or not and choosing when to modify the contrast C. In this context there are two natural generalizations to Eqn. (A5), both of which rely on some implicit "effective presentation interval" during which the subject attends to the stimulus to decide whether it is visible or not.

In the first formulation, which we will call the *constant T formulation*, the subject is assumed to study the stimulus for a fixed time T, independent of the flicker frequency. In the second formulation, the *constant N formulation*, we assume that the subject observes the stimulus for a fixed number of cycles, N, of the flickering. In both formulations we assume that after the observer adjusts the contrast he or she then ignores the stimulus for a

sufficiently long time that transients may be neglected and we can be assume that $R_j(t)$ is periodic.

But as the responses are assumed periodic there is, in both formulations, an issue about the point in the cycle of the periodic flickering at which the observer begins to attend to the stimulus. That is, there is some unknown phase $0 \leq \theta \leq 1$ such that the limits of the integral in (A5) become

$$T_0 = \theta/\nu \qquad \text{and} \qquad T_1 = \begin{cases} (\theta/\nu) + T & \text{In the constant } T \text{ formulation} \\ (\theta + N)/\nu & \text{In the constant } N \text{ formulation} \end{cases}$$

And as there is no way of knowing θ, one must average over all possible values, replacing the integral in the exponent of (A5) with, for example in the constant N formulation,

$$\begin{aligned} \int_0^1 d\theta \int_{\theta/\nu}^{(\theta+N)/\nu} \sum_{j=0}^{2} |A_j R_j(t)|^\beta \, dt &= \int_0^{N/\nu} \sum_{j=0}^{2} |A_j R_j(t)|^\beta \, dt \\ &= N \left[\int_0^{1/\nu} \sum_{j=0}^{2} |A_j R_j(t)|^\beta \, dt \right] \end{aligned} \tag{A6}$$

where, in simplifying the expression, we have used the fact that the integral of a periodic function over N complete periods is independent of starting time and equal to N times the integral over a single period. Notice that the final line is proportional to N, but that no N's appear inside the square brackets surrounding the integral: integrals over a single period of the responses $R_j(t)$ are all that need be computed.

In the constant T formulation the corresponding calculation is

$$\int_0^1 d\theta \int_{\theta/\nu}^{(\theta/\nu)+T} \sum_{j=0}^{2} |A_j R_j(t)|^\beta \, dt = \int_0^1 d\theta \int_0^T \sum_{j=0}^{2} |A_j R_j(s + \theta/\nu)|^\beta \, ds$$

where, in passing from the left hand side to the right, we have changed the variable of integration to $s = t - \theta/\nu$. Then, interchanging the order of integration, we obtain the following

$$\int_0^1 d\theta \int_0^T \sum_{j=0}^{2} |A_j R_j(s+\theta/\nu)|^\beta \, ds = \int_0^T ds \int_0^1 \sum_{j=0}^{2} |A_j R_j(s+\theta/\nu)|^\beta \, d\theta$$

To continue with this calculation it is convenient to make a second change of variable, defining $\eta = \theta/\nu$:

$$\begin{aligned} \int_0^T ds \int_0^1 \sum_{j=0}^{2} |A_j R_j(s+\theta/\nu)|^\beta \, d\theta &= \int_0^T ds \int_0^{1/\nu} \sum_{j=0}^{2} |A_j R_j(s+\eta)|^\beta \, \nu d\eta \\ &= \int_0^T \nu ds \int_0^{1/\nu} \sum_{j=0}^{2} |A_j R_j(s+\eta)|^\beta \, d\eta \end{aligned}$$

Finally, again using the fact that the integral of a periodic function over a complete period is independent of the starting point, we obtain:

$$\begin{aligned} \int_0^T \nu ds \int_0^{1/\nu} \sum_{j=0}^{2} |A_j R_j(s+\eta)|^\beta \, d\eta &= \int_0^T \nu ds \left[\int_0^{1/\nu} \sum_{j=0}^{2} |A_j R_j(\eta)|^\beta \, d\eta \right] \\ &= \nu T \left[\int_0^{1/\nu} \sum_{j=0}^{2} |A_j R_j(\eta)|^\beta \, d\eta \right] \end{aligned}$$

This result has a certain formal similarity to (A6): both results are proportional to the integral of $|R_j(t)|^\beta$ over a single period, but the fixed-T result includes a factor of the frequency ν that is absent from Eqn. (A6).

Armed with these results, it is easy to write down a probability of non-detection:

$$P(C, \nu : \tau, \sigma, \beta, \boldsymbol{A}) = \begin{cases} 2^{-\nu T \left[\int_0^{1/\nu} \sum_{j=0}^{2} |A_j R_j(\eta)|^\beta \, d\eta \right]} & \text{Constant } T \text{ formulation} \\ 2^{-N \left[\int_0^{1/\nu} \sum_{j=0}^{2} |A_j R_j(\eta)|^\beta \, d\eta \right]} & \text{Constant } N \text{ formulation} \end{cases} \tag{A7}$$

But these formulae are meant to be used as the basis for the maximum-likelihood fitting program outlined in Section A and, for this, they include too many parameters. To see why, consider the expression for the exponent in the constant N formulation:

$$\begin{aligned} N\left[\int_0^{1/\nu}\sum_{j=0}^{2}|A_jR_j(\eta)|^\beta\,d\eta\right] &= \sum_{j=0}^{2}N\left[\int_0^{1/\nu}|A_jR_j(\eta)|^\beta\,d\eta\right] \\ &= \sum_{j=0}^{2}N{A_j}^\beta\left[\int_0^{1/\nu}|R_j(\eta)|^\beta\,d\eta\right]. \end{aligned} \tag{A8}$$

The last line emphasizes the fact that the probability of non-detection depends only on the products $N{A_j}^\beta$, which means that if one were to change N to, say, $N' = \alpha N$ and, at the same time, change all the filter amplitudes to $A'_j = A_j/\alpha^{1/\beta}$ then the products that enter into (A8) would remain unchanged:

$$N'(A'_j)^\beta \;=\; (\alpha N)\left(\frac{A_j}{\alpha^{1/\beta}}\right)^\beta \;=\; (\alpha N)\left(\frac{{A_j}^\beta}{\alpha}\right) \;=\; N{A_j}^\beta$$

In other words, one cannot hope to find a unique, best-fitting set of parameters if one permits both N and the A_j to vary. Alternatively one could say that the expressions (A9) are unsuited to our data in the sense that, without further measurement, we cannot distinguish between a very deliberate observer who looks at the signal for a long time (has a large N or T), but has rather small filter amplitudes A_j, and a quicker observer who looks briefly (*i.e.*, has $N' << N$ or $T' << T$), but compensates with larger filter amplitudes A'_j.

To get rid of this ambiguity we fix one of the parameters, choosing $T = 1$ in the constant T formulation and $N = 1$ in the constant N formulation. This leads the following expressions,

which yield a well-posed, maximum-likelihood parameter-fitting problem:

$$P(C,\,\nu:\,\tau,\,\sigma,\,\beta,\,\boldsymbol{A}) = \begin{cases} 2^{-\nu\left[\int_0^{1/\nu}\sum_{j=0}^{2}|A_j R_j(\eta)|^\beta\,d\eta\right]} & \text{Constant } T \text{ formulation} \\ 2^{-\left[\int_0^{1/\nu}\sum_{j=0}^{2}|A_j R_j(\eta)|^\beta\,d\eta\right]} & \text{Constant } N \text{ formulation} \end{cases} \tag{A9}$$

These probabilities are the main ingredient required for the analysis in Section A.

Acknowledgments

The authors thank D. Carden and J. Simpson for their technical assistance; A.G. Robson for serving as observer; J.S. Werner, K.T. Mullen and K. Kranda for comments on earlier drafts; R.C. Baraas is funded by the Norwegian Research Council Grant 182768/V10.

Fig. 1. Spectral Sensitivity at 1 Hz as a function of wavelength is plotted for two observers, RB (a) and JK (b). The curves for bars are shifted down by one and two log units, for clarity. Top curves, marked by empty circles, are standard spectral sensitivity functions on a white background (3350 K) with its characteristic peaks. Intrusion of the luminance mechanism makes the notch shallower as is shown by spectral sensitivity curve on yellow background (2520 K), marked by filled circles. Elongation of test stimuli on a white background reduces spectral sensitivity in the blue range, only slightly for wide bars (empty squares) and more substantial for narrow bars (empty triangles). The 25 Hz homochromatic flicker function approximating the luminosity function is plotted for a narrow bar on white only (dotted line) for comparison. Spectral sensitivity for bars on yellow background (filled squares and triangles) increases in the blue range, as expected. Error bars are 1SD.

Fig. 2. Results for (a) blue (450 nm) and (b) yellow (574 nm) spot stimuli on yellow background as a function of Temporal Frequency [Hz]: the measured thresholds (for observer RB, JK and AG) are shown as solid dots and the predicted sensitivity curves for the best-fitting models in each class are shown as lines. The solid line represents model M_{01}; the dashed line model M_{02}; and the dash- dot line model M_{012}. The predicted sensitivity curves for the one-filter model M_0 gives the least likely fits (for details see third row of Tables 2, 3 and 5, 6), and are therfore not shown. The two-filter model M_{01} is the model that fits the data for the blue spot best, whereas it is the three-filter model M_{012} that fits the yellow spot best.

Fig. 3. Results for blue (450 nm) and yellow (574 nm) bar stimuli on white or yellow backgrounds as a function of Temporal Frequency [Hz]. Data (for observer RB): the conventions are as in Fig. 2. The two-filter model M_{01} fits the results for the blue bar best, whereas it is the three-filter model M_{012} that fits the yellow bar best.

Fig. 4. Results for blue (450 nm) and yellow (574 nm) bar stimuli on white or yellow backgrounds as a function of Temporal Frequency [Hz]. Data (for observer JK): the conventions are as in Fig. 2. The two-filter model M_{01} fits the results for the blue bar best, whereas it is the three-filter model M_{012} that fits the yellow bar best.

Fig. 5. Results for blue (450 nm) and yellow (574 nm) bar stimuli on white or yellow backgrounds as a function of Temporal Frequency [Hz]. Data (for observer AG): the conventions are as in Fig. 2. The two-filter model M_{01} fits the results for the blue bar best, whereas it is the three-filter model M_{012} that fits the yellow bar best.

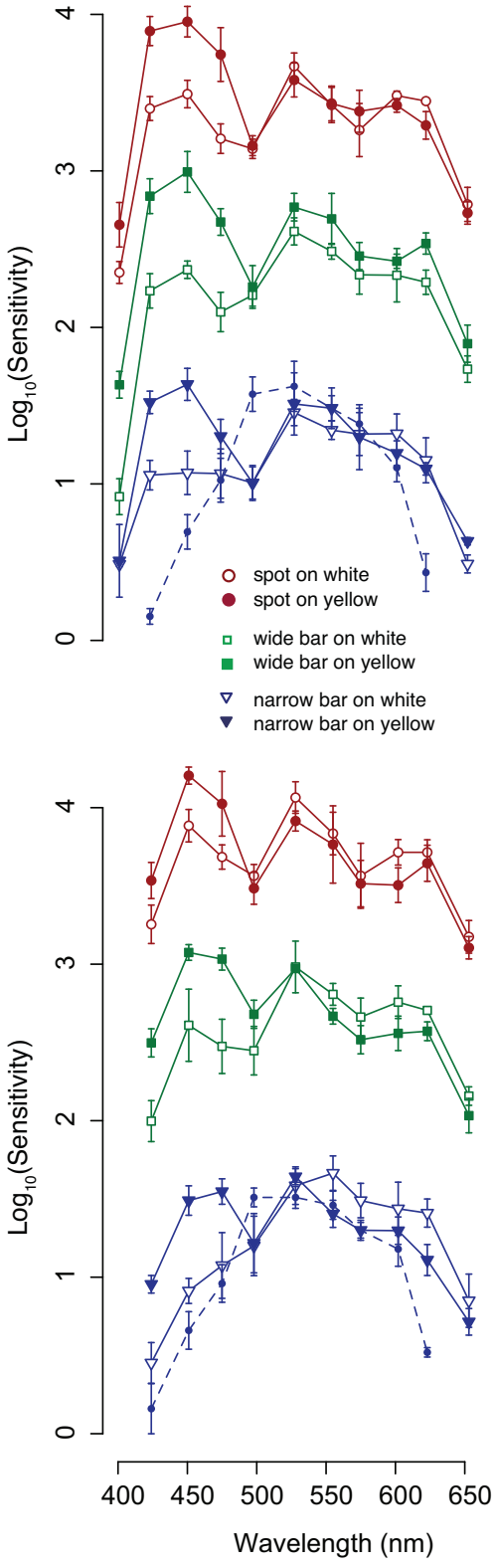
Log10(Sensitivity)
0
1
2
3
4
spot on white
spot on yellow
wide bar on white
wide bar on yellow
narrow bar on white
narrow bar on yellow
400
450
500
550
600
650
Wavelength (nm)

Figure 1.

Figure 2.

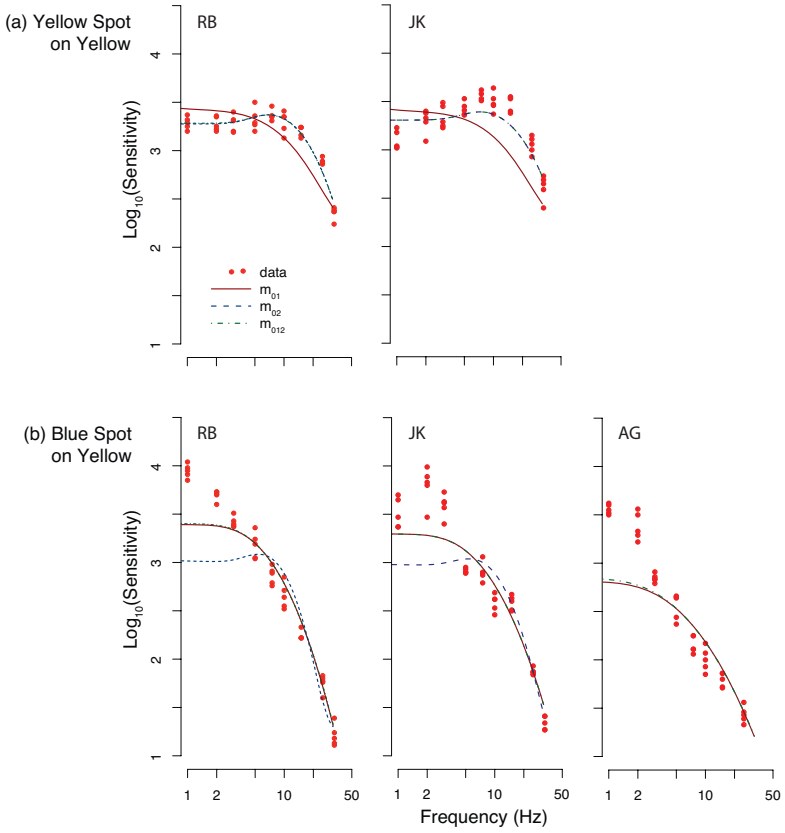
(a) Yellow Spot on Yellow
RB
JK
Log10(Sensitivity)
data
m01
m02
m012
(b) Blue Spot on Yellow
RB
JK
AG
Log10(Sensitivity)
1
2
3
4
1
2
10
50
Frequency (Hz)

Figure 3.

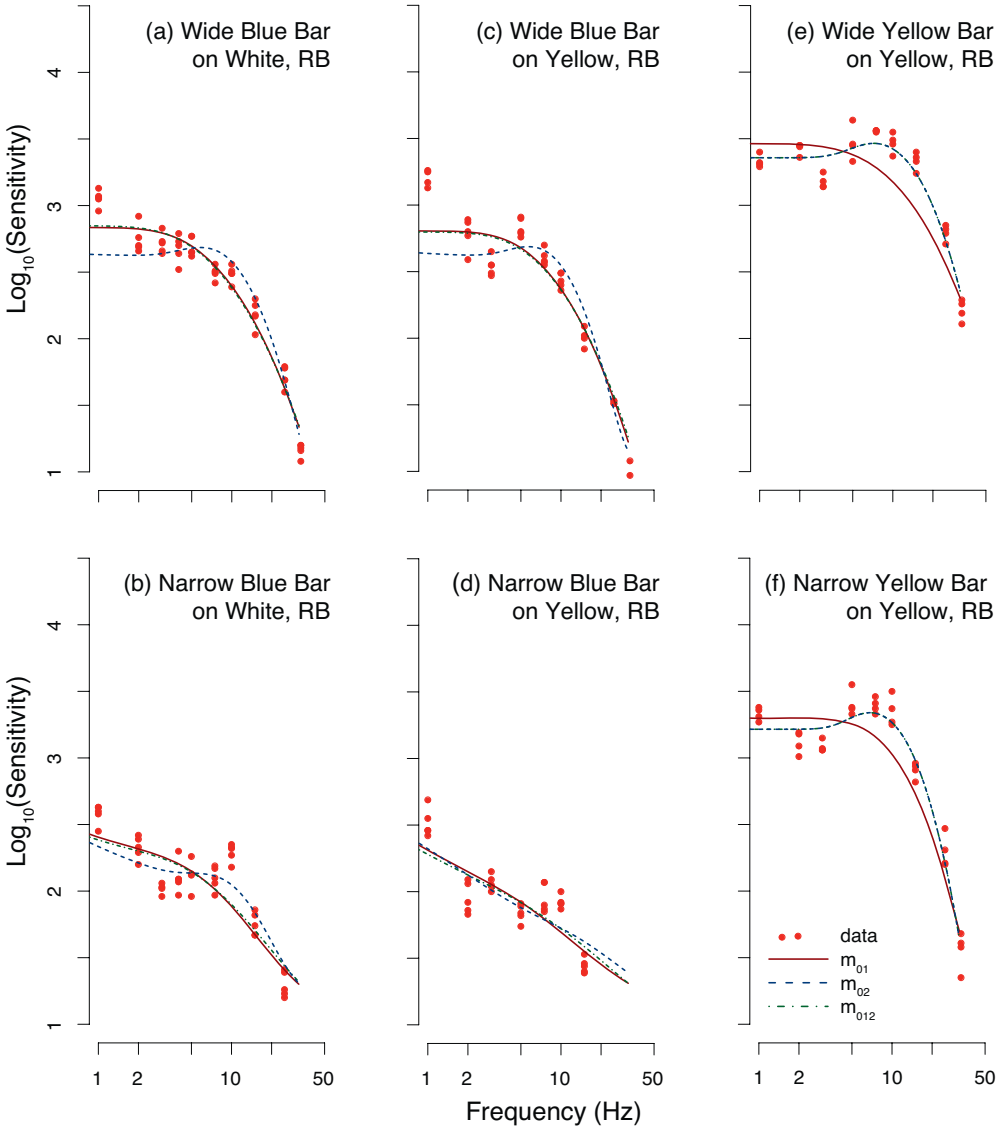
(a) Wide Blue Bar on White, RB
(c) Wide Blue Bar on Yellow, RB
(e) Wide Yellow Bar on Yellow, RB
(b) Narrow Blue Bar on White, RB
(d) Narrow Blue Bar on Yellow, RB
(f) Narrow Yellow Bar on Yellow, RB
Log10(Sensitivity)
Frequency (Hz)
1
2
3
4
1
2
10
50
data
m01
m02
m012

Figure 4.

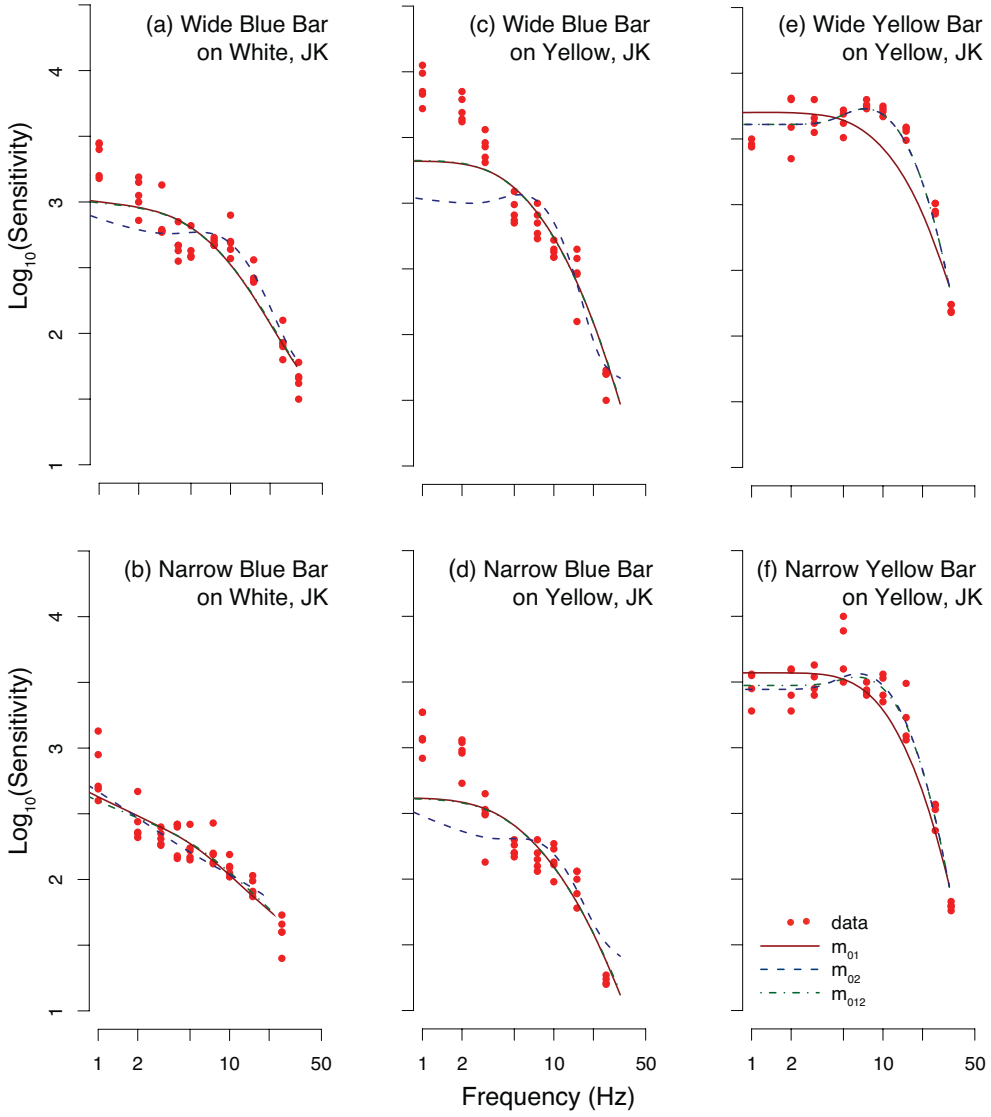
(a) Wide Blue Bar on White, JK
(c) Wide Blue Bar on Yellow, JK
(e) Wide Yellow Bar on Yellow, JK
(b) Narrow Blue Bar on White, JK
(d) Narrow Blue Bar on Yellow, JK
(f) Narrow Yellow Bar on Yellow, JK
Log10(Sensitivity)
Frequency (Hz)
1
2
3
4
1
2
10
50
data
m01
m02
m012

Figure 5.

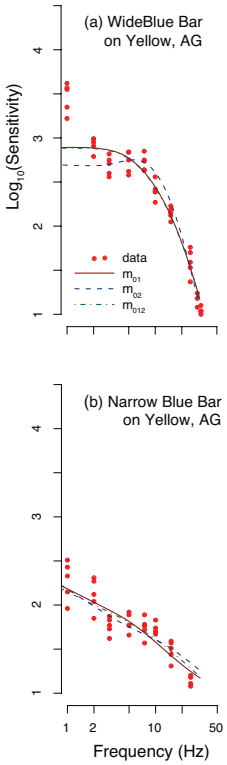
(a) WideBlue Bar
on Yellow, AG
Log10(Sensitivity)
1
2
3
4
data
m01
m02
m012
(b) Narrow Blue Bar
on Yellow, AG
1
2
3
4
1
2
10
50
Frequency (Hz)

Table 1. Parameters of the Gaussian priors on the parameters τ and σ. Note that the prior (4) depends on the features $f_j(\tau, \sigma)$, which were evaluated numerically.

Feature $f_j(\tau, \sigma)$	m_j	s_j
$f_0(\tau, \sigma)$: freq. at half-maximal gain for the low-pass filter	8 Hz.	3 Hz.
$f_1(\tau, \sigma)$: freq. at peak gain for the 1st band-pass filter	4 Hz.	1 Hz.
$f_2(\tau, \sigma)$: freq. at peak gain for the 2nd band-pass filter	14 Hz.	3 Hz.

Table 2. Results for blue (450 nm) stimuli on white or yellow backgrounds for observer RB: for each type of stimulus, the total likelihood score of the best model is italicized. The column headed p_1 gives the p-values with regards to whether each of the two-filter or three-filter models is more likely than the one-filter model M_0. The column headed p_2 gives the p-values with regards to whether each of the two-filter models, M_{01} or M_{02}, is more likely than the three-filter model M_{012}. The two-filter model M_{01} has a small numerical edge over the other models in four out of five conditions, but is not significantly different from the three-filter model M_{012}.

Stimulus	**Model**	**Prior**	**Fit**	**Total**	p_1	p_2
Wide blue bar	M_0	-8.26	-118.55	-126.81		
on white	M_{01}	-8.24	-70.77	*-79.01*	< 0.01	
	M_{02}	-13.29	-74.43	-87.72	< 0.01	
	M_{012}	-8.17	-70.95	-79.12	< 0.01	> 0.99
Narrow blue bar	M_0	-8.02	-71.95	-79.97		
on white	M_{01}	-8.09	-68.21	-76.30	< 0.01	
	M_{02}	-12.28	-65.47	-77.75	0.04	
	M_{012}	-8.10	-68.10	*-76.20*	0.02	0.65
Blue spot	M_0	-8.26	-169.28	-177.54		
on yellow	M_{01}	-14.53	-73.31	*-87.84*	< 0.01	
	M_{02}	-16.14	-95.51	-111.65	< 0.01	
	M_{012}	-14.83	-73.04	-87.87	< 0.01	> 0.99
Wide blue bar	M_0	-8.26	-98.37	-106.63		
on yellow	M_{01}	-8.82	-59.48	*-68.30*	< 0.01	
	M_{02}	-14.52	-61.52	-76.04	< 0.01	
	M_{012}	-8.53	-59.80	-68.33	< 0.01	> 0.99

Table 3. Results for blue (450 nm) stimuli on white or yellow backgrounds for observer JK: for each type of stimulus, the total likelihood score of the best model is italicized. The conventions are as in Tabel 2.

Stimulus	**Model**	**Prior**	**Fit**	**Total**	p_1	p_2
Wide blue bar	M_0	-8.10	-91.99	-100.09		
on white	M_{01}	-8.02	-76.66	*-84.68*	< 0.01	
	M_{02}	-12.44	-77.16	-89.60	< 0.01	
	M_{012}	-8.02	-76.63	-84.65	< 0.01	0.81
Narrow blue bar	M_0	-8.02	-65.58	-73.60		
on white	M_{01}	-8.02	-64.53	*-72.55*	0.15	
	M_{02}	-8.05	-65.50	-73.55	0.75	
	M_{012}	-8.02	-64.50	-72.52	0.34	0.81
Blue spot	M_0	-8.26	-148.16	-156.42		
on yellow	M_{01}	-10.72	-76.15	*-86.87*	< 0.01	
	M_{02}	-15.03	-91.31	-106.34	< 0.01	
	M_{012}	-10.72	-76.15	-86.87	< 0.01	> 0.99
Wide blue bar	M_0	-8.26	-113.93	-122.19		
on yellow	M_{01}	-12.36	-70.50	*-82.86*	< 0.01	
	M_{02}	-16.19	-85.62	-101.81	< 0.01	
	M_{012}	-12.56	-70.32	-82.88	< 0.01	> 0.99
Narrow blue bar	M_0	-8.10	-81.04	-89.14		
on yellow	M_{01}	-8.63	-66.80	*-75.43*	< 0.01	
	M_{02}	-13.77	-73.56	-87.33	0.06	
	M_{012}	-8.53	-66.97	-75.50	< 0.01	> 0.99

Table 4. Results for blue (450 nm) stimuli on white or yellow backgrounds for observer AG: for each type of stimulus, the total likelihood score of the best model is italicized. The conventions are as in Tabel 2.

Stimulus	**Model**	**Prior**	**Fit**	**Total**	p_1	p_2
Blue spot	M_0	-8.26	-95.31	-103.57		
on yellow	M_{01}	-11.18	-77.37	*-88.55*	< 0.01	
	M_{02}	-8.26	-95.31	-103.57	> 0.99	
	M_{012}	-12.33	-76.24	-88.57	< 0.01	> 0.99
Wide blue bar	M_0	-8.26	-146.22	-154.48		
on yellow	M_{01}	-9.76	-76.34	*-86.10*	< 0.01	
	M_{02}	-14.57	-81.79	-96.36	< 0.01	
	M_{012}	-9.76	-76.36	-86.12	< 0.01	> 0.99
Narrow blue bar	M_0	-8.02	-58.64	-66.66		
on yellow	M_{01}	-8.02	-58.02	-66.04	0.27	
	M_{02}	-8.02	-58.23	-66.25	0.37	
	M_{012}	-8.02	-57.74	*-65.76*	0.41	0.45

Table 5. Results for yellow (574 nm) stimuli on yellow background for observer RB: for each type of stimulus, the likelihood score of the best model is italicized. The conventions are as in Table 2. The three-filter model M_{012} has a small numerical edge over the simpler models in two out of three conditions, but is not significantly different from the two-filter model M_{02}.

Stimulus	**Model**	**Prior**	**Fit**	**Total**	p_1	p_2
Yellow spot	M_0	-10.14	-100.88	-111.02		
on yellow	M_{01}	-10.90	-75.64	-86.54	< 0.01	
	M_{02}	-10.75	-62.31	-73.06	< 0.01	
	M_{012}	-10.75	-62.30	*-73.05*	< 0.01	0.89
Wide yellow bar	M_0	-8.52	-107.09	-115.61		
on yellow	M_{01}	-10.14	-68.53	-78.67	< 0.01	
	M_{02}	-12.19	-52.62	-64.81	< 0.01	
	M_{012}	-12.19	-52.60	*-64.79*	< 0.01	0.84
Narrow yellow bar	M_0	-9.05	-178.20	-187.25		
on yellow	M_{01}	-12.52	-65.58	-78.10	< 0.01	
	M_{02}	-13.82	-53.36	*-67.18*	< 0.01	
	M_{012}	-13.82	-53.36	-67.18	< 0.01	> 0.99

Table 6. Results for yellow (574 nm) stimuli on yellow background for observer JK: for each type of stimulus, the likelihood score of the best model is italicized. The conventions are as in Table 2.

Stimulus	**Model**	**Prior**	**Fit**	**Total**	p_1	p_2
Yellow spot	M_0	-11.11	-121.52	-132.63		
on yellow	M_{01}	-13.80	-104.08	-117.88	< 0.01	
	M_{02}	-9.61	-72.44	*-82.05*	< 0.01	
	M_{012}	-9.61	-72.45	-82.06	< 0.01	> 0.99
Wide yellow bar	M_0	-9.25	-138.16	-147.41		
on yellow	M_{01}	-10.86	-66.87	-77.73	< 0.01	
	M_{02}	-13.43	-51.35	*-64.78*	< 0.01	
	M_{012}	-13.43	-51.35	-64.78	< 0.01	> 0.99
Narrow yellow bar	M_0	-9.05	-170.64	-179.69		
on yellow	M_{01}	-11.96	-60.53	-72.49	< 0.01	
	M_{02}	-13.73	-54.41	-68.14	< 0.01	
	M_{012}	-13.51	-54.31	*-67.82*	< 0.01	0.42